Polymorphic, Porous and Host-Guest Nanostructures Directed by Monolayer-Substrate Interactions: Epitaxial Self-Assembly Study of Cyclic Trinuclear Au(I) Complexes on HOPG at the Solution-Solid Interface

Bhaskar Chilukuri,*[,†] Roy N. McDougald Jr.,[‡] Mukunda M. Ghimire,[‡] Vladimir N. Nesterov,[‡] Ursula Mazur,[†] Mohammad A. Omary,*[,‡] and K. W. Hipps,*[,†]

[†]Department of Chemistry, Washington State University, Pullman, WA 99164-4630, USA.
[‡]Department of Chemistry, University of North Texas, Denton, TX 76203, USA.

(S) *Supporting Information*

ABSTRACT: Synthesis, crystallographic characterization and molecular self-assembly of two novel cyclotrimeric gold(I) complexes, $Au_3[3,5\text{-}(COOEt)_2Pz]_3$ (Au_3Pz_3) and $Au_3[(n\text{-}Pr\text{-}O)C{=}N(Me)]_3$ (Au_3Cb_3) was studied. Single crystal X-ray crystallography data reveal that both gold(I) complexes have 1-dimensional stacking patterns caused by intermolecular Au(I)···Au(I) aurophilic interactions. The Au_3Pz_3 trimer units stack with two alternate and symmetrical Au(I)···Au(I) interactions while the Au_3Cb_3 units have three alternating and non-symmetrical Au(I)···Au(I) interactions. Molecular self-assembly of the gold(I) complexes on the 1-phenyloctane/highly ordered pyrolytic graphite (HOPG) (0001) solution-solid interface is studied with scanning tunneling microscopy (STM). The gold(I) cyclotrimers form epitaxial nanostructures on the HOPG surface. At a concentration of ~1×10^{-4} M, Au_3Pz_3 complexes exhibit a single morphology, while Au_3Cb_3 complexes exhibit polymorphology. Two polymorphs, one non-porous and the other porous, are observed at 22.0 ±2.0 °C for Au_3Cb_3 complexes. A non-porous, low-surface-density (0.82 molecules/nm^2) Au_3Cb_3 nanostructure forms first then transforms into a high-density (1.43 molecules/nm^2) porous nanostructure. This is the first time any porous surface nanostructure is reported for an organometallic system. The porous structure is thought to be stabilized by a combination of hydrogen bonding and monolayer-substrate interactions. These pores are utilized to incorporate pyrene into the film, rendering this the first organometallic host-guest system imaged at the solid-solution interface. Molecular and periodic density functional theory (DFT) calculations shed light on the two-dimensional topography and polymorphic self-assembly revealed by STM; these calculations suggest significant electronic hybridization of the Au_3 trimer orbitals and HOPG. The multiple-technique approach used herein provides insights concerning molecule-substrate and molecule-molecule interactions.

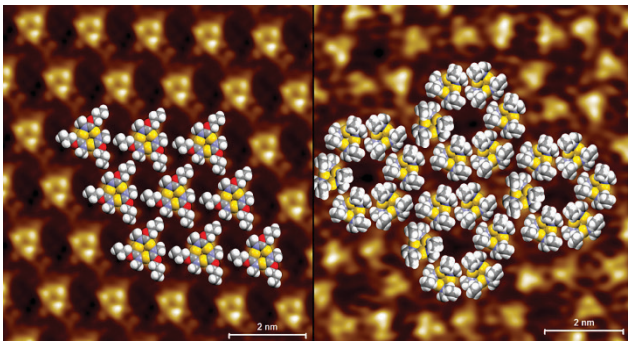

1. INTRODUCTION

Self-assembly of molecules is recognized as an encouraging strategy for surface functionalization and 'bottom up' fabrication of devices.[1,2] Controlled deposition/growth of molecules leads to a variety of model nanostructures yielding promising applications in molecular electronics, nano-lithography, sensors, molecular sieves, catalysis, etc.[2,3] Molecular self-assembly processes can be controlled by a number of experimental variables, including molecule concentration,[4] temperature,[5] environment, mode of deposition etc.[6-9] The morphology of molecules/nanostructures on surfaces can also be controlled by a variety of interactions including covalent, dipole-dipole, van der Waals, hydrogen bonding, specific adsorbate-surface interactions, and surface packing forces.[7,8,10] Understanding the types of interactions in molecular assemblies on surfaces is essential for controlling the self-assembly process through the careful design of building blocks. It also promotes the discovery of novel fabrication strategies.

Scanning tunneling microscopy (STM) is an excellent tool for probing chemical interactions, electronic properties and morphology of molecules on surfaces.[1-**Error! Bookmark not defined.**,11] STM studies in the past were typically performed in ultrahigh vacuum (UHV) conditions.[12,13] Recently, numerous STM studies have been performed at the solution-solid (SS) interface,[14-16] opening up new areas of study concerning dynamic adsorption/desorption at the surface.[17,18] Solution-solid interface studies not only provide an important facet of fundamental science but also help solve problems related to practical applications. STM studies of molecular self-assembly of organic and biological molecules[19-21] are becoming more common, but similar studies on organometallic complexes are comparatively scant. In part, this is due to their complex molecular structures which are generally not flat. Thus, when placed on conductive substrates it is usually the organic components of the metal-organic complex that drive the morphology. . Most STM self-assembly studies on organic systems containing transition metals are generally on

complexes such as metalloporphyrins[14] and metal-phthalocyanines,[22] where the organic backbone and its substituents are as important, or more important, to the molecular self-assembly as/than the particular transition metal. In fact, with the exception of possible axial coordination of the metal ions, the significant properties are often defined by the organic structure. STM studies of self-assembly of non-porphyrin/phthalocyanine metal-organic complexes are not prevalent. The corresponding literature search yields only a few studies, most of which were described in excellent reviews by Barth and co-workers.[2,23]

A variety of strategies have been employed to tune the molecular self-assembly of metal-organic complexes on surfaces. These strategies include metallosupramolecular architectures using adatoms,[24-26] metal co-deposition, host-guest interactions,[6] sequential deposition of metal-ligand tectons,[27,28] molecular grid-like structures,[29] *etc*. These STM studies were performed both at UHV and at SS-interfaces with the former more prevalent than the latter. It was noted[2,23] that by appropriately choosing the transition metals, ligands and substrates, one can obtain and control a host of surface morphologies, topographies and functionalizations, that may yield potential scientific and technological applications. Hence, understanding the influence of metals on molecular self-assembly should be of immense interest considering they can provide a different set of molecular and supramolecular interactions *viz.*, metal-metal bonding, metal-substrate and metal-ligand interactions that could strongly influence the self-assembly process. In particular, incorporating *d* and *f* orbitals into adsorbates may significantly modify both the chemical and electronic properties of the resulting adlayer.

Among the many STM studies of self-assembly of metal-organic species, studies on gold-containing complexes are extremely rare. To our knowledge, the only studies reported in the literature include gold cyanide molecules on Au(111),[30,31] gold atom clusters on HOPG,[32] gold nanoparticles[33-35] and Au^{+3} porphyrins[36] on Au(111), and Au_6 nanoclusters on TiO_2.[37,38] There is only one report of a self-assembly of gold containing metal-organic species.[39]

In this manuscript we report the self-assembly of two new cyclic trinuclear complexes (CTCs), comprising gold(I) pyrazolate (Au_3Pz_3) and carbeniate (Au_3Cb_3) cyclotrimers (Scheme 1), on the HOPG surface. Similar CTCs reported in the literature are synthesized via monovalent coinage metals.[40,41] The CTCs have a flat geometry (roughly D_{3h}) with multiple modes of *metallophilic* interactions revealed in their crystal packing, which imparts a wide spectrum of interesting properties including π-acidity and π-basicity, tunable photoluminescence, solvoluminescence (spontaneous luminescence upon solvent contact), field-effect properties, chemisorptive removal of hazardous vapor, *etc*.[42-44] These fascinating optoelectronic properties allow for their use in potential applications in sensing, optical, and electronic devices.

Recently, a great deal of interest has been shown in the functionalization of epitaxial graphene (EG) for device applications.[45,46] It was reported that the doping of EG can help in controlling the charge carrier type of the material.[47] Functionalization of EG with organic molecules is one of the strategies used for control of charge carriers.[48-50] Molecules used for functionalization should electronically couple to graphene and this is generally most effective if the electron donor/acceptor is flat. CTCs, due to their flat structure and tunable charge carrier properties,[43,51] can be excellent candidates for the functionalization of graphene and other carbon nanostructures. Hence determination of surface morphology and properties of CTCs on graphene or graphene-like surfaces should be of great interest. As a first step, HOPG, which is essentially multilayer graphene sheets, is used as a substrate to study the morphology and properties of CTCs .

Scheme 1 Molecular Structures of gold(I) cyclic trinuclear complexes.

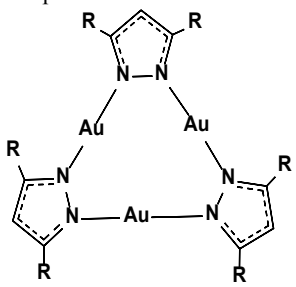

Au_3[3,5-$(COOEt)_2Pz$]$_3$/Au_3Pz_3
R = –$COOC_2H_5$

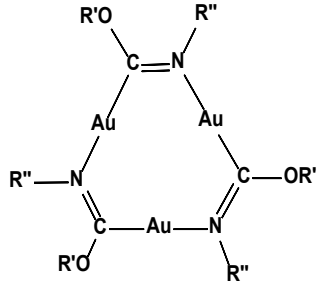

Au_3[(*n*-Pr-O)C=N(Me)]$_3$ /Au_3Cb_3
R' = –(n-C_3H_7), R''= –CH_3

Surface studies of CTCs are very rare, and the only such precedent we are aware of is the STM study of gold(I) pyrazolate at the octanoic acid/HOPG interface by the Swager group.[39] In that work, AuPz trimers with long-chain (C12 and C18) alkyl substituents self-assemble in various morphologies that are concentration dependent. Additionally, at high concentrations (> 10^{-4} M), gold(I) CTCs dimerized on the surface forming a monolayer with multiple domains, which undergo time-dependent transit into a single domain due to cooperative dynamics.[39] The long-chain C12 and C18 substituents on the gold(I) pyrazolate trimers played a crucial role in the assembly of the 2D surface pattern. Contrary to the earlier precedent,[39] the new trimers reported here have short alkyl, alkoxy, and ester substituents. Thus, the adsorption properties are more controlled by the trimer itself rather than the long-chain substituents. The structures herein are also well-defined such that their crystal structures are determined by single crystal X-ray diffraction, which also allows for accurate modeling of their molecular and supramolecular structures via molecular and periodic DFT simulations. Long-chain substituents in such Au trimers, in contrast, tend to form less ordered structures such as liquid crystals and organogels that are usually characterized by powder XRD instead.[52] Furthermore, the new materials should provide a much greater net charge transfer to the graphene surface because of the higher density of trimer molecules per unit area.

The current study is unique in several aspects. First, the STM study of any gold(I) carbeniate complex is reported for the first time. Second, this is the only study whereby any genuinely organometallic gold complex (with Au-C bonds)

is used to form metal-directed porous surface nanostructure. Third, this is the only STM study of a self-assembled organometallic host-guest system ever reported on a surface. The use of small alkyl substituents gives a much clearer view of the role of the metallocyclic trimeric core in the self-assembly process. And finally, DFT calculations, in agreement with STM imaging, demonstrate very strong Au-HOPG electronic interactions.

2. EXPERIMENTAL SECTION

A. Synthesis and physical measurements: The methyl isocyanide ligand is synthesized from a previously reported literature procedure,[53] whereas the 3,5-diethylpyrazoledicarboxylate ligand is purchased from Sigma Aldrich. The chloro(tetrahydrothiophene)gold(I), Au(THT)Cl, starting material is synthesized based upon a reported literature procedure.[54] The solvents *n*-propanol, acetonitrile, tetrahydrofuran (THF) and dichloromethane (DCM), are distilled by conventional drying agents and degassed with argon, prior to use. All glassware is oven-dried at 150 °C overnight, prior to use. All manipulations were carried out under an atmosphere of purified argon gas using standard Schlenk techniques.

The ^{1}H and ^{13}C NMR spectra were recorded in deuterated chloroform ($CDCl_3$) at ambient temperature on a Varian nuclear magnetic resonance (NMR) spectrometer operating at 500 MHz. The samples were dissolved in $CDCl_3$ using approximately 15 to 20 mg of complex in 0.75 mL of solvent and placed in a standard NMR tube. The chemical shifts in the ^{1}H and ^{13}C NMR spectra are reported relative to tetramethylsilane in $CDCl_3$. Fourier Transform Infrared (FTIR) spectroscopic experiments were completed on a Thermo Scientific Nicolet 6700 FTIR with a Smart Orbit diamond attenuated total reflectance (ATR) accessory. The spectra were collected by firmly pressing the neat sample on to the diamond plate of the ATR attachment. Melting point (M.P.) determinations for each compound were completed with an Electrothermal Mel-Temp melting point apparatus.

Compound I, $Au_3[3,5\text{-}(COOEt)_2Pz]_3$ (Au_3Pz_3): The preparations of $Au_3[3,5\text{-}(COOEt)_2Pz]_3$ are completed from procedures reported previously for the methyl-substituted analogue.[55] Into an evacuated 50 mL Schlenk flask 0.20 g (0.62 mM) of Au(THT)Cl and 131 mg (0.62 mM) of diethyl-3,5-pyrazoledicarboxylate are dissolved and stirred in 10 mL of dry THF at room temperature. 35 mg (0.62 mM) of potassium hydroxide dissolved in 1 mL of dry MeOH is added drop wise to the stirring solution. The resulting solution is allowed to continue stirring for one hour, after which the solvent is then evaporated under reduced pressure. The remaining solid is dissolved in a minimum amount of THF and precipitated by adding excess acetonitrile. The final product is filtered and allowed to dry under vacuum overnight. Purification is accomplished by recrystallization from THF and acetonitrile. $Au_3[3,5\text{-}(COOEt)_2Pz]_3$: M.P. 215 °C (dec.). Yield 68%, IR spectrum: ν(N=N) 1529 cm^{-1}, ^{1}H NMR (δ in $CDCl_3$): 4.420, 1.389 , and 7.516 ppm. ^{13}C NMR (δ in $CDCl_3$): 143.859, 160.155, 61.607, and 14.648 ppm.

Compound II, $Au_3[(n\text{-Pr-O})C{=}N(Me)]_3$ (Au_3Cb_3): The preparations of $Au_3[(n\text{-Pr-O})C{=}N(Me)]_3$ follow procedures reported previously for $Au_3[(MeO)C{=}N(Me)]_3$.[56] Into an evacuated 50 mL Schlenk flask 0.03 mL (0.62 mM) of methyl isocyanide and 35 mg (0.62 mM) of potassium hydroxide are dissolved in 15 mL of dry *n*-propanol. The resulting solution is stirred for 30 minutes at 0 °C, in an ice bath. Then 0.20 g (0.62 mM) of Au(THT)Cl is added to the stirring solution, and the solid starting material slowly dissolves. The resulting solution is allowed to continue stirring for 1 hour at 0 °C, after which the solvent is then evaporated under reduced pressure. The remaining solid is dissolved in a minimum amount of DCM and filtered through a bed of Celite in order to remove any decomposed material and salt by-products. The solvent is again evaporated under reduced pressure, leaving a crude white material. Recrystallization of this crude material is completed by dissolving the complex in a minimum amount of DCM, adding excess acetonitrile and filtering the precipitating white solid. The final product is allowed to dry under vacuum overnight. $Au_3[(n\text{-Pr-O})C{=}N(Me)]_3$: M.P. 125 °C while decomposition occurs at 193 °C. Yield 65%. IR spectrum (pure powder): ν(C=N) 1564 cm^{-1}, ^{1}H NMR (δ in $CDCl_3$): 4.351, 1.714, 0.934, and 2.963 ppm. ^{13}C NMR (δ in $CDCl_3$): 199.225, 73.945, 23.359, 10.337, and 39.217 ppm

B. Structure Determination of I and II by X-ray Crystallography: Crystal structure determination for both complexes were carried out using a Bruker SMART APEX2 CCD-based X-ray diffractometer equipped with a Mo-target X-ray tube (wavelength = 0.71073 Å). Data collection was completed at 100(2) K. Data collection, indexing, and initial cell refinements were carried out using APEX2,[57] frame integration and final cell refinements were done using SAINT.[58] A multiple absorption correction was applied using the program SADABS.[59] All non-hydrogen atoms were refined anisotropically. The hydrogen atoms in the complexes were placed in idealized positions and were refined as riding atoms. In **I** the largest residual electron density was located close to (less than 0.8 A ° from) Au atoms and was most likely due to imperfect absorption corrections frequently encountered in heavy-metal atom structures. Structure solution, refinement, graphic and generation of publication materials were performed by using SHELXTL software.[60]

C. STM sample preparation and measurements: Reagent grade dichloromethane (DCM) was purchased from J.T. Baker. Phenyloctane (99%) was purchased from Sigma Aldrich. All reagents were used without further purification. The 1 cm^2 HOPG substrates (grade 2) were purchased from SPI supplies, West Chester, PA. STM images were recorded using a Molecular Imaging (now Agilent) Pico Plus STM equipped with a 1×1.5 μm^2 head and an environmental chamber. STM tips were made by cutting or electrochemically etching $Pt_{0.8}Ir_{0.2}$ wire from California Fine Wire Company Grover Beach, CA. Images were typically obtained at a sample bias of +0.9 and −0.5 V, and a tunneling current of 20 and 40 pA. Scan rates typically were 4.9 lines/sec.

Stock solutions 20 ml each of Au_3Pz_3 (**I**) and Au_3Cb_3 (**II**) were prepared by dissolving suitable amounts of compounds in DCM and/or phenyloctane solvents to make the solution concentration 1 mM. The stock solutions were then diluted to a concentration of 100–300 μM each in DCM or phenyloctane. STM samples were prepared by dropping a 15 μL aliquot of the 100 μM solution on a freshly peeled 1 cm^2 HOPG substrate. In the case of DCM solution, the solvent is allowed to evaporate and the dried surface was then covered with 15 μl droplet of phenyloctane, and the resulting sample was then placed on the STM stage. In the case of phenyloctane solution, the STM sample is prepared by dropping the respective solution on HOPG substrate and scanned without any solvent evaporation. The resulting surface structures show no dependence on sample preparation method. Imaging is commenced immediately and all images were recorded while scanning at the phenyloctane/HOPG solution-solid interface. All STM images were background subtracted and non-linearity corrected using SPIP image processing software[61] and drift corrected using a linear drift correction algorithm.[62]

Pyrene solution was prepared to determine whether it can act as a guest with the hexagonal porous morphology of Au_3Cb_3 (Figure 4c-d, 5) being the host. Suitable amounts of pyrene crystals purchased from Sigma Aldrich were dissolved in phenyloctane to make the solution concentration 500 μM. A 10 μL aliquot of the pyrene solution is added on top of previously self-assembled and scanned sample of CS morphology of Au_3Cb_3 in the solution cell/reservoir. At the aforementioned solution concentrations and volume the pyrene to Au_3Cb_3 mole ratio is found to be 3.33:1.

3. COMPUTATIONAL SECTION

A. Molecular Modeling: The Gaussian 09 package[63] is used to perform density functional calculations. Los Alamos valence basis sets, LANL2DZ(2*f*,*p*)* [64] (with augmented d-polarization functions taken from 6-31G* basis set on main group elements) are employed in conjunction with the M06 functional[65] for all optimization and single point calculations. The extended basis set was used, particularly on the gold atoms augmented by two *f* functions[66] and one Couty-Hall outer p function.[67] Calculations with the M06 functionals gave results consistent with available experimental data and consistent with previous calculations on similar CTC systems to solve problems that have often required accounting for dispersion-like forces.[42,44,68]

The goal of the molecular modeling simulations is to determine the gas-phase molecular orbital (MO) mappings and to develop optimized molecular models for use in the two dimensional lattice drawings based on experimental STM images. Unsubstituted Au_3Pz_3 and Au_3Cb_3 molecular models (Figure S17 in SI) were generated and optimized using aforementioned DFT methodology. Unsubstituted models of Au_3Pz_3 and Au_3Cb_3 were used for simplicity due to numerous possibilities of substituent alignment as seen in the crystal structure (Figure 1) and due to very low barriers of rotation for alkyl chain substituents. Both Au_3Pz_3 and Au_3Cb_3 molecules have degenerate highest occupied molecular orbitals (HOMO) and one delocalized lowest unoccupied molecular orbital (LUMO), Figure 2A-B. The HOMOs have significant density around the gold(I) atoms and some density on the ligands, while the LUMO is delocalized at the trinuclear center.

B. Periodic Modeling Methodology: All simulations were performed using the Vienna Ab initio Simulation Package (VASP)[69-71] version 5.2. Periodic calculations were performed using plane-wave density functional theory (PW-DFT) within the projector augmented wave (PAW) method[72,73] to describe the core electrons and valence–core interactions. All calculations were performed with dispersion corrected vdW-DF[74,75] functional of Klimes, Langreth and Lundqvist *et al.* which takes into account the nonlocal nature of electron correlation. The functional used is the optB88-vdW GGA functional[76] with PBE potentials having *p*, *s* semicore valence for Au atoms. It was previously reported[77] that calculations with dispersion corrected vdW-DF functional yields better geometries and properties in contrast to experiment than with conventional hybrid DFT functionals. For slab calculations, the electronic wave functions are sampled in a *k*-point grid of 2×2×1 in the irreducible Brillouin zone (BZ) using the Monkhorst and Pack (MP)[78] method. Isolated Au_3Pz_3, Au_3Cb_3 molecules were sampled with only a gamma point. A plane wave cut off energy of 550 eV was used for all simulations and this value is determined from energy convergence tests on HOPG primitive lattices. Methfessel–Paxton smearing was used to set the partial occupancies for each wave function with a smearing width of 0.2 eV. Finally, band decomposed charge densities and constant current STM images were simulated using the Tersoff-Hamann[79,80] approach implemented in the bSKAN code.[81] This code uses the electron wavefunctions of the slab computed previously with VASP.

4. RESULTS AND DISCUSSION

A. X-ray Crystallography of Gold Cyclotrimer Complexes.

Crystallographic Characteristics of $Au_3[3,5\text{-}(COOEt)_2Pz]_3$: Colorless crystals of this Au_3Pz_3 complex were grown by slow evaporation of a tetrahydrofuran solution of the complex, which formed long needles. The single crystal X-ray data collection and model refinement details are summarized in Table 1. This complex crystallizes in the monoclinic *P21/c* space group, wherein a tight extended-chain of trimers exists. Each of the diethylcarboxylpyrazolate bridging ligands lies perpendicular to the plane of the Au_3Pz_3 core nine-membered ring. The intramolecular Au···Au distances are 3.3611(4), 3.3986(4) and 3.3945(4) Å. Figure 1 (top right) shows the molecules interact to form an extended-chain arrangement along the *a*-axis. Each of the molecules forms two Au···Au contacts with the molecule above and two with the molecule below, yielding a total of four Au···Au intermolecular interactions, with alternating Au···Au distances of 3.273 and 3.492 Å. This motif of alternating

short Au···Au contact distances allows for an extended-chain interaction between the molecules. Other distances and angles are given in the supporting information, Table S1. It is important to note here that when the X-ray analysis for the same needle was collected at 200 K, the Au···Au intertrimer distances increased to 3.321 and 3.493 Å while further heating to 298K attained further expansion to 3.387 and 3.534 Å. Thus, upon proceeding from 100 K to room temperature (298 K), the shorter Au···Au contact extended by 0.114 Å while the longer contact lengthened by 0.042 Å. This shows a tendency for an equilibration between the two alternating distances as a function of temperature.

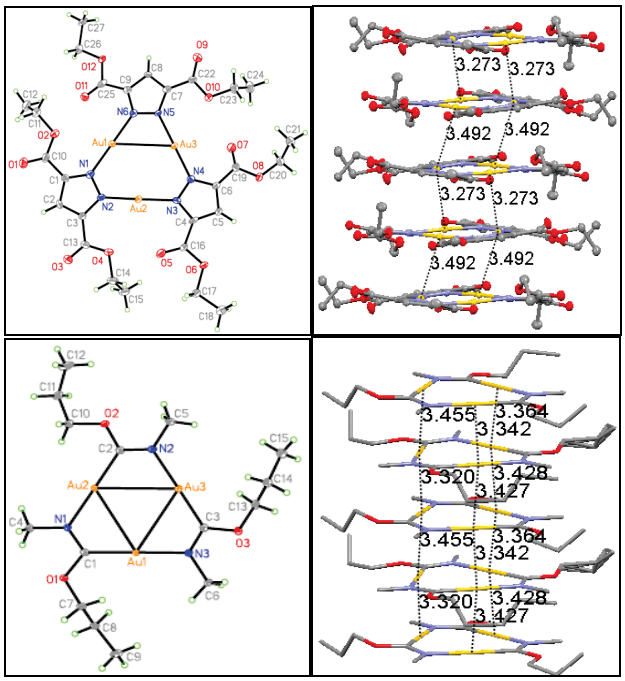

Figure 1. Crystal structures of gold CTCs. Left: Thermal ellipsoid diagrams for a single molecule of $Au_3[3,5\text{-}(COOEt)_2Pz]_3$ (top) and $Au_3[(n\text{-}Pr\text{-}O)C{=}N(Me)]_3$ (bottom). Right: Packing diagrams showing the intermolecular interactions between molecules in the crystal structures of $Au_3[3,5\text{-}(COOEt)_2Pz]_3$ (top) and $Au_3[(n\text{-}Pr\text{-}O)C{=}N(Me)]_3$ (bottom). Hydrogen atoms are omitted for clarity. Atom color codes: yellow = Au, blue = N, gray = C, red = O.

Crystallographic Characteristics of $Au_3[(n\text{-}Pr\text{-}O)C{=}N(Me)]_3$: Colorless crystals of this Au_3Cb_3 complex were grown by slow diffusion from the layering of acetonitrile on a dichloromethane solution of the complex, resulting in the formation of long needles. This complex crystallizes in the monoclinic *C2/c* space group and exhibits a stacking pattern akin to Balch's hexagonal polymorph of the methoxy/methyl analogue, $Au_3[(MeO)C{=}N(Me)]_3$;[82] *i.e.*, the individual planar molecules aggregate along the *c*-axis to form extended trigonal-prismatic stacks. The Balch hexagonal polymorph[82] stacks with the C atoms and N atoms of the ligand aligned throughout the prismatic stacks; for $Au_3[(n\text{-}Pr\text{-}O)C{=}N(Me)]_3$, the extended chains contain alternating C and N atoms. The stacking motif between trimers shows Au···Au contacts between 3.320 and 3.455 Å. The monoclinic needles of $Au_3[(n\text{-}Pr\text{-}O)C{=}N(Me)]_3$ have three trinuclear complexes in the asymmetric unit. The single crystal X-ray data collection and model refinement details are summarized in Table 1. All three of the *n*-propyl groups lie parallel to the plane of the Au_3Cb_3 core nine-membered ring. The intramolecular Au-Au distances are 3.2982(3), 3.3117(3), and 3.3119(3) Å. Other bond distances and angles are given in the supporting information, Table S1. As anticipated, the center geometry of the nine-membered Au_3Cb_3 ring in this trinuclear complex is similar to that of the $Au_3[(MeO)C{=}N(Me)]_3$ complex.[82] Figure 1 (bottom right) shows the molecules interact to form an extended-chain arrangement along the *b*-axis. Each of the molecules in the crystal forms three Au···Au contacts with one molecule above and with one molecule below. This gives rise to a total of six short Au···Au intermolecular interactions with distances of 3.320, 3.342, 3.364, 3.427, 3.428, and 3.455 Å.

Table 1. Crystallographic data for $Au_3[3,5\text{-}(COOEt)_2Pz]_3$ and $Au_3[(n\text{-}Pr\text{-}O)C{=}N(Me)]_3$.

	$Au_3[3,5\text{-}(COOEt)_2Pz]_3$	**$Au_3[(n\text{-}Pr\text{-}O)C{=}N(Me)]_3$**
Crystal System	Monoclinic	Monoclinic
Color/Habit	colorless needle	colorless needle
Formula	$C_{27}H_{33}Au_3N_6O_{12}$	$C_{15}H_{30}Au_3N_3O_3$
Formula weight	1224.49	891.32
Space group	P 2(1)/c	C 2/c
a, (Å)	7.8205(11)	45.158(3)
b, (Å)	16.240(2)	6.7542(4)
c, (Å)	24.953(3)	25.332(2)
α, (deg)	90	90
β, (deg)	93.029(2)	91.291(1)
γ, (deg)	90	90
V, (Å^3)	3164.8(7)	8334.2(9)
Z	4	16
T, (K)	100(2)	100(2)
λ, (Å)	0.71073	0.71073
ρ_{calc}, (mg/m^3)	2.570	2.841
μ, (cm^{-1})	13.946	21.089
*R*1 [$I > 2\sigma(I)$]	0.0252	0.0172
*wR*2 [$I > 2\sigma(I)$]	0.0615	0.0404
*R*1 (all data)	0.0330	0.0208
*wR*2 (all data)	0.0662	0.0417

B. Scanning Tunneling Microscopy (STM) of Gold Cyclotrimer Complexes.

Scanning tunneling microscopy (STM) images (Figures 3 and 4) of gold CTCs on graphite at the solution–solid interface indicate that gold trimers form a uniform monolayer on graphite. The solvent used at the solid–solution interface is phenyloctane. Both Au_3Pz_3 and Au_3Cb_3 molecules appear bright at the trinuclear centers. Despite the formal +1 oxidation state and filled d^{10} shell in both Au(I) CTCs, gold atoms are the predominant contributors to the overall bright appearance in the STM images. Within the considered bias range (+1 to -1 V), STM images of gold CTCs show bright trinuclear centers (Figures 3 and 4). This

finding is interesting because the topography of the STM images is *not consistent* with the calculated (Figure 2A-B) highest occupied (HOMO) and lowest unoccupied (LUMO) molecular orbitals of isolated Au_3Pz_3 (Figure 2a) and Au_3Cb_3 (Figure 2B) molecules obtained using molecular DFT calculations. As can be seen by comparing experiment (Figures 3 and 4) with calculations (Figure 2a, 2b), gold atoms are always the predominant contributors to STM topography in experiment. In the calculations on isolated molecules, however, it can be seen that there is significant contribution from the ligand (Pz_3 or Cb_3) orbitals to the HOMO and LUMO that is delocalized at the center of the Au_3 trimer rings -- instead of contributions from gold atoms alone. This observation is further corroborated by molecular orbitals (band energy decomposed charge density) and density of states (DOS) obtained using periodic DFT calculations on isolated Au_3Pz_3 (Figure 2c) and Au_3Cb_3 (Figure 2d) molecules, and with literature.[42,68]

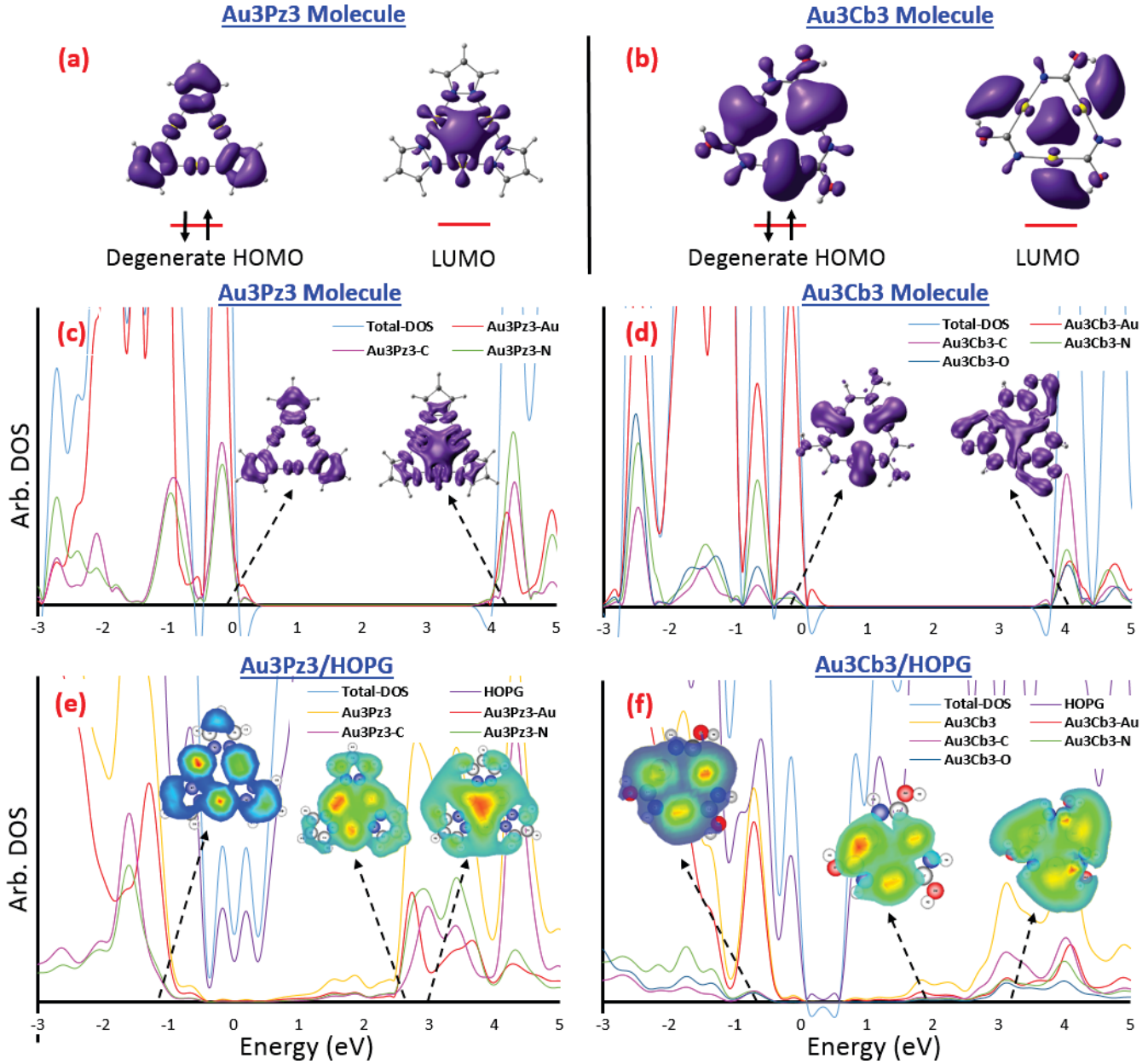

Figure 2. Frontier molecular orbitals mappings of Au_3Pz_3 (a) and Au_3Cb_3 (b) molecules obtained from molecular DFT calculations. Density of states (DOS) and band decomposed charge densities at specified energies of isolated Au_3Pz_3 (c) and Au_3Cb_3 (d) molecules and Au_3Pz_3/HOPG (e) and Au_3Cb_3/HOPG (f) interfaces obtained from periodic DFT calculations. The Fermi energies (E_f) for each DOS plot in figures C-F are adjusted to zero eV.

We attribute the predominance of gold character in the STM topography of Au_3 trimers on HOPG to strong interactions between the Au_3Pz_3 or Au_3Cb_3 monolayers on the one hand and the HOPG substrate on the other hand, hence attaining significant electronic hybridization of the orbitals of Au_3 trimers and HOPG. The hybridization can be clearly seen when we compare the DOS of isolated molecules of Au_3Pz_3 (Figure 2c) or Au_3Cb_3 (Figure 2d) with those for Au_3Pz_3/HOPG (Figure 2e) or Au_3Cb_3/HOPG (Figure 2f) interfaces, respectively. Additionally, we plotted

the calculated STM images using band decomposed charge density and the Tersoff-Hamann method[79,80] at specific energies of the valence and conduction bands. It can be clearly seen that when the Au_3 trimers are placed on HOPG, at bias voltages near the top of the valence band (at -1.2 eV in Figure 2e or at -0.8 eV in Figure 2f), gold atom contributions to the DOS become more predominant than ligand contributions -- contrary to the situation for the CTCs *without* the HOPG substrate (at -0.3 eV in either of Figure 2c or Figure 2d). Similarly, at the bottom of conduction band (at 2.7 eV in Figure 2e and at 1.8 eV in Figure 2f), gold atom contributions to the DOS are highly predominant -- again contrary to the situation *without* the HOPG substrate wherein the contributions to the DOS are localized at the center of the Au_3 trimer (at 4.2 eV in Figure 2C and at 4.0 eV in Figure 2d). Note that the delocalized LUMO/DOS seen in the non-bound Au_3Pz_3 trimer (at 4.2 eV in Figure 2c) is still present in the HOPG-bound molecule (near 3.0 V in Figure 2c), but it is no longer the lowest unoccupied state. A similar result is seen for Au_3Cb_3 in Figures 2d and 2f. This difference clearly demonstrates significant orbital hybridization at the trimer-HOPG interface. The strong electronic hybridization of Au_3 trimers when on HOPG may have occurred due to strong correlation and relativistic effects of the Au(I) atomic clusters.[83]

All STM images of Au_3Pz_3 and Au_3Cb_3 molecules on HOPG were obtained from solution concentrations and volumes which are 100 times more than necessary to provide a single monolayer of molecules on 1 cm^2 HOPG substrate, thus ensuring the avoidance of any island formation. Note that irrespective of the solvent (either DCM or 1-phenyloctane) used for the solution preparation, there is always a reservoir of phenyloctane in the solution cell (see STM sample preparation in experimental section). There is a natural partitioning of Au3 complexes between solution and surface such that a multilayer never forms. The free energy change associated with multilayer formation is much more positive than that of solution,

STM of $Au_3[3,5\text{-}(COOEt)_2Pz]_3$: STM images of $Au_3[3,5\text{-}(COOEt)_2Pz]_3$ or Au_3Pz_3 reveal that CTC molecules form a uniform monolayer on HOPG with molecules lying flat on the surface (Figure 3a). Each molecule lies at an intermolecular center-to-center distance of 1.59±0.05 nm (Figure S6) from its neighbors. The flat orientation of the trinuclear metallocycle on the surface is enhanced by the strong d_π-C_π interactions (Figure 2e) between Au_3Pz_3 molecules and the HOPG substrate. Similar interactions were also suggested in a computational study of Au_3Pz_3 molecules on Au(111).[84] The bright appearance of Au_3Pz_3 molecules on HOPG provides experimental evidence of the computed electronic coupling between the HOPG and CTC π systems.

An important facet of this study, which has implications toward a variety of applications, is the resolution of the surface structure of Au_3Pz_3 monolayer. STM images were able to clearly resolve the positions of the gold atoms but not the pyrazolate ligand and ester substituents of the Au_3Pz_3 molecule. Hence, we utilize the molecular geometry of Au_3Pz_3 obtained from the crystal structure and DFT calculations to develop a molecular model structure (see Sec. I in the Supporting Information, SI). A correctly-scaled molecular model of Au_3Pz_3 is overlaid on a high-resolution (drift, non-linear corrected) STM image on graphite in Figure 3b.

Utilizing the molecular model, two-dimensional intermolecular center-center distances, and Au_3Pz_3 orientation with respect to the HOPG step edges (see Sec. II and Figure S4 in the SI), we have mapped the surface lattice structure of Au_3Pz_3 monolayer on HOPG. It was found that gold pyrazolate molecules self-assemble in a 2-D hexagonal lattice with one molecule per unit cell, $a = b = 1.54$ nm and $\alpha = 60^o$ (Figure 3c). Also, this self-assembly follows an epitaxial pattern with monolayer unit cell vectors A = $2a_1+7a_2$ and B = $7a_1+5a_2$, where a_1, a_2 are graphite lattice vectors. Note that the length of the epitaxial Au_3Pz_3 hexagonal lattice (1.54 nm) is slightly shorter than the measured intermolecular center-center distances (1.59±0.05 nm), yet within the error range. The epitaxial unit cell is chosen by making the structure consistent with the orientation of the Au_3Pz_3 trimers with respect to the step edge (see Sec. II and Figure S4 in SI). Within the epitaxial lattice sites, the density of the Au_3Pz_3 monolayer on HOPG is calculated to be 0.487 molecules/nm^2.

Au_3Pz_3 molecules on HOPG have very interesting 2D morphological features. Although STM imaging could not resolve the geometry of the pyrazolate ligand and ester substituents of the Au_3Pz_3 molecules, we hypothesize that the ethyl ester substituents lie, along with oxygen atoms of the -COO groups, flat and parallel to the HOPG surface (Figures 3b-c). This hypothesis can be justified based on three factors. First, the observed intermolecular distances of neighboring Au_3Pz_3 molecules would be much shorter if ethyl substituents were facing up above the HOPG surface -- rather than being parallel. Second, Au_3Pz_3 adsorption on HOPG would have been much weaker and dynamic if oxygen atoms were not flat on the surface because any rotation from the flat geometry of the –COO group would increase the distance between the Au_3Pz_3 metallocycle and the HOPG surface. Finally, the third reason for the flat orientation of substituents is the very low rotational barriers (~ 4 kcal/mole)[85] of the ethylester groups on the pyrazolate ligands in solution. Hence, the molecular model used to construct the proposed 2-D unit cell of Au_3Pz_3 monolayer on HOPG can be justified. At this point, it is important to note that periodic DFT calculations of unsubstituted Au_3Pz_3 molecules on Au(111) surface have shown that the pyrazolate ligands tend to bend away from the surface by ~10^o while gold atoms in Au_3Pz_3 bind strongly to the surface.[84] We anticipate the $Au_3[3,5\text{-}(COOEt)_2Pz]_3$ molecules to lie predominantly flat even on the Au(111) surface due to their ester substituents.

The correlation average of the STM image (Figure 3b), indicates that the gold trimers are all oriented in the same direction. However, careful inspection of the original data (inset in Figure 3a) suggests deviations from this orientation. It can be clearly seen that Au_3Pz_3 trimers can occur in an inverted orientation (60° rotation) relative to their neighbors. We refer to such orientations as defects in

the monolayer. With or without the defect in the orientation, Au_3Pz_3 trimers fit the same unit cell parameters (Figures 3c-3d) with no intermolecular collisions. An important contrast between the current case and the previous study[39] of C12- and C18- substituted gold(I) pyrazolates is that the current Au_3Pz_3 molecules do not dimerize at high concentration ($\geq 10^{-4}$ M) even after 36 hours post deposition. Presumably, the interaction with the HOPG surface (*vide supra*) is so strong such that it possibly hinders intertrimer Au···Au association.

The 2D packing in the STM image of Au_3Pz_3 trimers has two similarities to its x-ray crystal structure. First, the lateral center-to-center distances in the STM (Figure 3) are consistent with the highly-ordered 2-D lattice plane in the crystal structure (Figure S1 in SI). Second, in the 2D lattice plane of the crystal structure, the Au_3Pz_3 trimers are rotated with respect to their neighbors in alternate rows. Similar rotations in Au_3Pz_3 trimers can be observed in STM images as well. We referred (*vide supra*) to such structures as defects in the STM images (Figures 3a and 3d). Finally, we also performed periodic DFT calculations to determine the possible binding site of Au_3Pz_3 molecules on HOPG. Details of the modeling methodology and calculations setup can be found in the computational methodology Sec. 3B above and in the SI, Sec. III and Figure S18, respectively. Periodic DFT calculations indicate that Au_3Pz_3 trimers prefer to bind to the HOPG surface at the C-C bridge site with the centroid of the trimer lying at the center of the bridge.

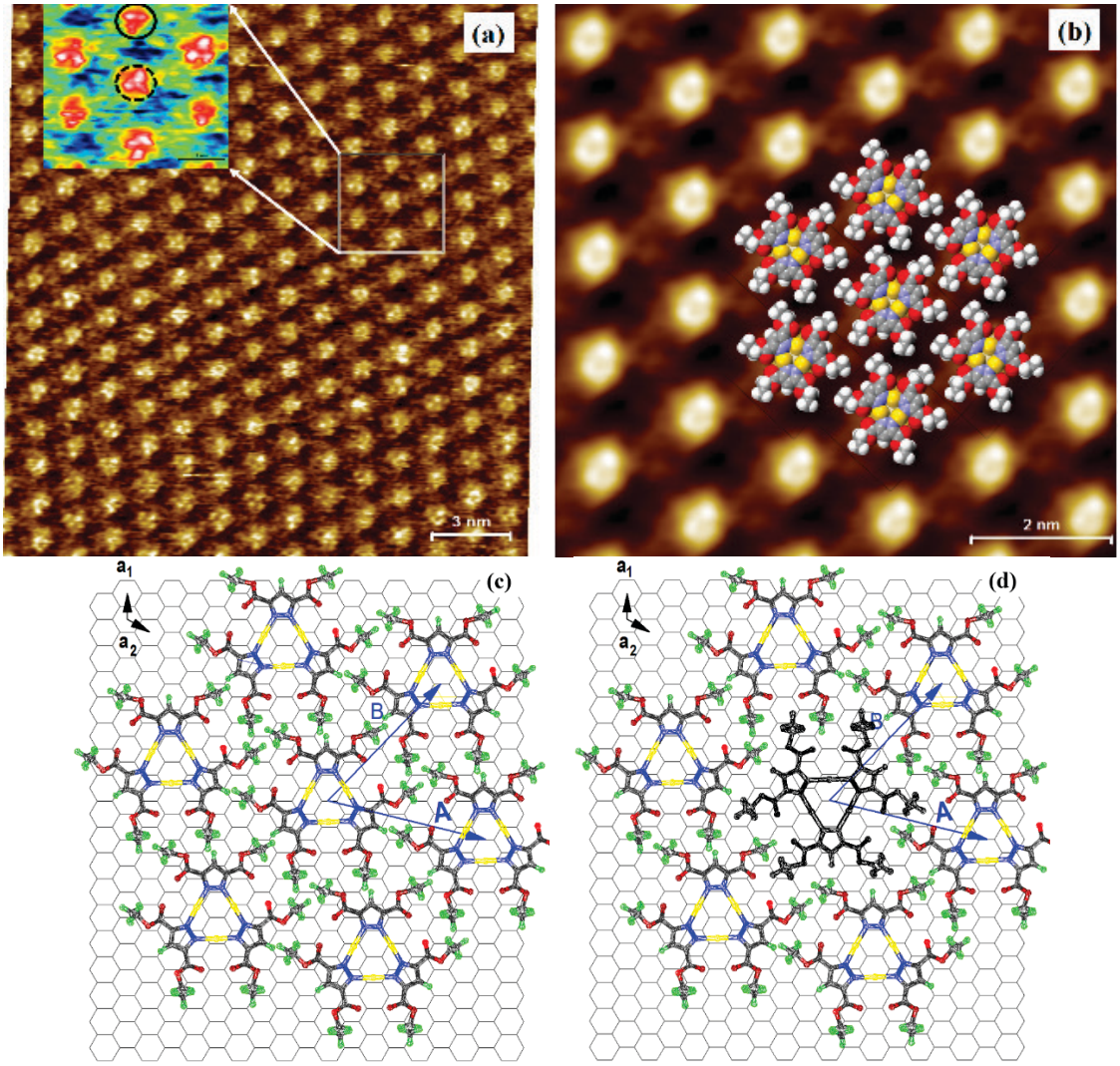

Figure 3. (a) STM image (+0.9 V bias and 40 pA setpoint) of an Au_3Pz_3 monolayer on HOPG; inset shows a zoomed image with inverted/defect trimers shown in solid/dotted circles. (b) A correlation-averaged STM image with models of Au_3Pz_3 laid on top. (c) A proposed 2D unit cell of Au_3Pz_3 monolayer on HOPG. (d) A proposed unit cell of an Au_3Pz_3 monolayer with a defect in black.

STM of Au_3[(n-Pr-O)C=N(Me)]$_3$: The second complex studied was the Au_3[(*n*-Pr-O)C=N(Me)]$_3$ complex (Au_3Cb_3). This complex also forms a monolayer with molecules lying flat on the HOPG surface. Similar to Au_3Pz_3, gold atoms appear brighter in the STM images than the ligands/substituents. Interestingly, there appears to be a polymorphic self-assembly of Au_3[(*n*-Pr-O)C=N(Me)]$_3$ molecules on HOPG. The first morphology (Figures 4a-4b) involves a monolayer with each Au_3Cb_3 molecule separated from its neighbor by 1.48±0.05 nm. In the second morphology (Figures 4c-4d), Au_3Cb_3 molecules assemble in the form of a hexagon wherein the center of each gold trimer is located at each vertex of the hexagon and the center of the hexagon has a vacant space, overall giving rise

to a porous structure with a pore diameter of ~ 9.5 Å. Each gold trimer within the hexagon is separated from its nearest neighbor at a center-to-center distance of 1.00±0.02 nm. For simplicity and comparison, we named the first morphology (Figures 4a-4b) as an "open structure (OS)" and the second morphology (Figures 4c-4d) as a "closed structure (CS)". When 2-D packing of OS and CS morphologies of Au_3Cb_3 trimers (Figure 4) are compared with the highly-ordered 2-D lattice plane in the crystal structure (Figure S2 in SI), we notice that the CS morphology has no obvious similarities with the crystal structure. On the other hand, the inter-trimer lateral center-to-center distances observed in OS are close to those found in the crystal structure, at least in one direction. Also we find that each Au_3Cb_3 trimer rotates with respect to its neighbor in the crystal structure, whereas no such rotations are observed in the OS morphology. Further structural details of OS and CS morphologies are discussed below. Initial observations and comparisons of the OS and CS morphologies lead to the following conclusions: First, both OS and CS morphologies are observed at a temperature of 22.0±2.0 ºC and with the same solution concentration of 1.0×10^{-4} M. Second, the open structure is formed first upon Au_3Cb_3 solution deposition on HOPG and it eventually transforms to a closed structure. Two consecutive images showing OS and CS are depicted in Figure S13 (SI). Third, the CS can be observed even at very low (~ 1 μM) solution concentrations, Figure S14 (SI). Fourth, the CS monolayer is the high-density structure (1.43 molecules/nm^2) while the OS monolayer has a low density of 0.82 molecules/nm^2. Surface density for OS and CS are determined based on the lattice structures (*vide infra*).

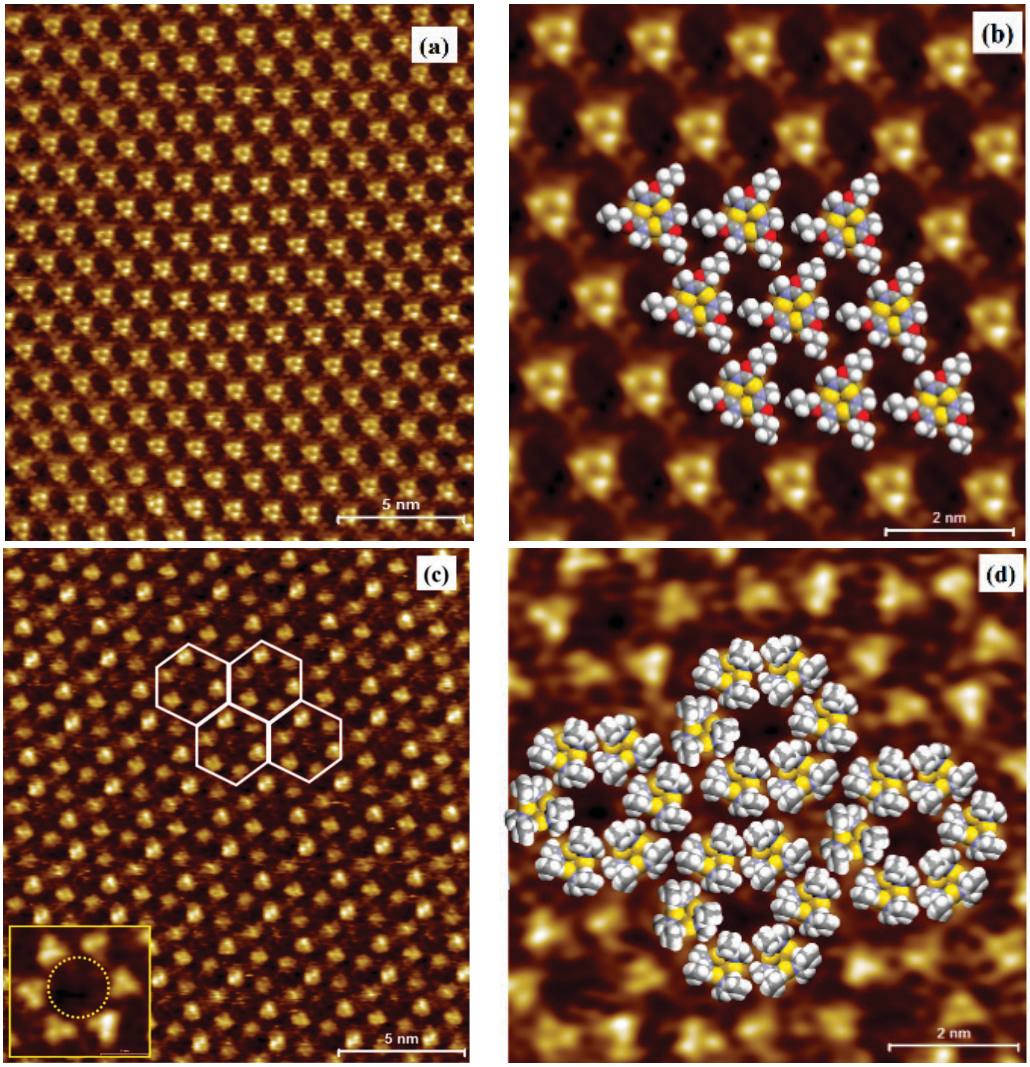

Figure 4. (a) STM image (-0.7 V and 40 pA setpoint) of an open structure (OS) Au_3Cb_3 monolayer on HOPG. (b) A correlation averaged OS STM image with models of Au_3Cb_3 laid on top. (c) A STM image (+0.5 V and 20 pA setpoint) of a closed structure (CS) Au_3Cb_3 monolayer on HOPG. The white hexagons represent each unit cell; inset at the bottom left corner represents high-resolution image of each CS while the dotted circle represents a nano-pore. (d) A correlation-averaged CS STM image with models of Au_3Cb_3 laid on top. Empty pores can be clearly seen at the center of each CS.

We also observed that capturing the transformation process from OS to CS during all STM scans was challenging and not always feasible. Sometimes the closed structure is observed immediately as we commence scanning (~10 minutes after sample deposition on HOPG substrate), indicating that transformation might have

occurred very quickly. However, we note that for the few instances we have were able to scan the morphology transformation (Figure S13, SI), we always observed the OS-to-CS transformation, but never the opposite, under the applied experimental conditions. What triggers the OS-to-CS transformation and how quickly this occurs is presently unknown. Temperature, solvent, and concentration are all likely to play a role in determining which polymorph is observed. More targeted studies are necessary to study the transformation process and will be performed in the future.

Generally, the more dense structure (CS in the current study) is expected to be the more stable structure[14] and is likely the thermodynamically-stable one because of the apparent irreversibility of the transition (at least for observation periods of up to 36 hours at 22°C). The OS is apparently kinetically more favorable, but the barrier to transformation to the CS must be on the order of *kT*. Similar transformations have been observed on other surface nanostructures such as those involving coronene,[86] alkylated dehydrobenzo-[12]annulene (DBA),[87] 1,3,5-tristyrylbenzene (TSB)[88] 1,3,5-tris(4-carboxyphenyl) benzene (BTB)[15] networks, *etc*. There are some interesting distinctions between the polymorphs formed from trigonal organic molecules and those of the organometallic Au_3Cb_3. For example, the hexagonal structure of DBA[87] is the low-density structure rather than the high-density one seen for Au_3Cb_3. In the case of BTB,[15] the pores close with increasing temperature while the pore phase is the more stable (at 22°C) in the Au_3Cb_3 nanostructure. The pore structure in BTB is also a low density structure similar to DBA[87] rather than the high-density one seen for Au_3Cb_3. Long alkyl chains or strong hydrogen bonding moieties were used to develop the long-range ordering in DBA and BTB, respectively. In contrast, weak hydrogen bonding and Au-HOPG interactions play a critical role (*vide infra*) in the formation of the porous structure of Au_3Cb_3.

The OS monolayer of Au_3Cb_3 (Figures 4a-4b) has the gold atoms of the trimers pointing in the same direction and no orientational defects are observed as in the Au_3Pz_3 (Figure 3d). Since the STM imaging of OS did not resolve the ligand and substituents in Au_3Cb_3 molecules, molecular models (see Sec. I, SI) based on the crystal structure and DFT calculations were developed and scaled to overlay the high-resolution open structure STM images (Figure 4b). The molecular models used in the overlay on the OS STM images (Figure 4b) have all propyl substituents lying flat and parallel to the HOPG surface in order to maximize the intermolecular center-to-center distances (1.48±0.05 nm) of the CTCs. However, in CS morphology, the trimers lie much closer (1.48±0.05 nm), so in order to rationalize the CS morphology, the alkane chains must be turned up away from the surface and into solution. This is possible because the *n*-propyl substituents on the carbeniate ligands of $Au_3[(n\text{-Pr-O})C{=}N(Me)]_3$ have a high flexibility due to very low rotational barriers of alkoxy groups (~ 3 kcal/mole).[89] The flat and non-flat orientations of *n*-propyl substituents in OS and CS can be corroborated by the correctly scaled molecular models shown Figures 4b and 4d, respectively. The molecular models used for OS and CS morphologies can be justified using the similar hypothesis proposed in the molecular model development for Au_3Pz_3 on HOPG (*vide supra*). In the current study and in the one reported in the literature[39] n-alkyl substituents on CTCs couldn't be resolved via STM. However, logical predictions can be made based on the intermolecular center-to-center distances of CTCs and how the n-alkyl substituents must orient to allow that packing (Figure 4b, 4d). All attempts to turn down the alkane chains were incompatible with the observed structures.

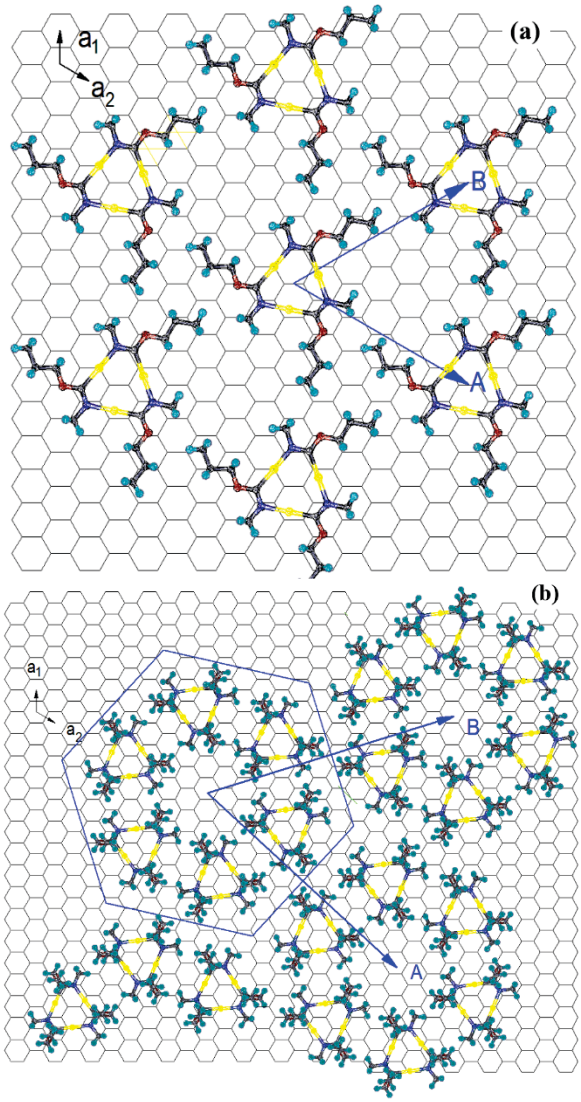

Figure 5. (a) Proposed unit cell of open structure (OS) Au_3Cb_3 monolayer on HOPG. (b) Unit cell of closed structure (CS) Au_3Cb_3 monolayer on HOPG.

Utilizing molecular models (see section I in SI), 2-D intermolecular center-to-center distances (Figures S8, S10-11 in SI) and the Au_3Cb_3 orientation with respect to the HOPG step edge (see Sec. II and Figure S4 in SI), we have mapped the surface lattice structures of OS and CS Au_3Cb_3 monolayer on HOPG. We find that gold carbeniate molecules self-assemble in a 2-D hexagonal lattice for both OS and CS morphologies (Figure 5). The OS morphology is formed in a hexagonal lattice with one molecule per unit cell, $a = b = 1.48$ nm and $\alpha = 60°$ (Figure 5a). We are

assuming that OS self-assembly follows an epitaxial pattern. However, we were unable to obtain the orientation of the OS with respect to the HOPG step edge. As a consequence, we have two equally probable epitaxial structures rotated by 34.70° with respect to one another. One such epitaxial structure is depicted in Figure S9 (SI), having monolayer unit cell vectors A = $6a_1+6a_2$ and B = $6a_2$, where a_1 and a_2 are graphite lattice vectors. Periodic DFT calculations (Sec. 3B in computational methods above and Sec. III and Figure S19 in SI) indicate that Au_3Cb_3 trimers prefer to bind to the HOPG surface at the C-C bridge site with the centroid of the trimer lying at the center of the bridge. However, in the case of porous CS morphology (Figure 5b), it can be seen that some trimers are centered at the C-C bridge site of HOPG while most of them are not. However, the CS orientation can be justified if the intermolecular and substrate interactions of Au_3Cb_3 molecules in CS are dominant and can compensate than the relatively small energy differences (~ 0.2 eV, Figure S19) when bound to different sites on HOPG.

The CS monolayer, which forms upon transformation from OS, has Au_3Cb_3 molecules assembled in a '*water wheel*' shape (inset in Figure 4c). The gold trimers are packed very closely (~10 Å intermolecular center-to-center distances, Figure S10 in SI) in the CS morphology. The 2-dimensional unit cell of the CS morphology is also formed in a hexagonal lattice with six molecules per unit cell, $a = b$ = 2.90 nm and α = 60º (Figure 5b). This self-assembly follows an epitaxial pattern with monolayer unit cell vectors A = $-3a_1+10a_2$ and B = $-10a_1+13a_2$. The '*water wheel*' shape and a six molecule hexagonal lattice of the CS is similar to that observed for 4-nitroaniline self-assembly on Au(111).[90] The close packing of the gold trimers can mostly be attributed to three factors. First, rotations of the *n*-propyl substituents of the carbeniate ligands, which are facing up above the surface of the monolayer towards the phenyloctane solution. Second, very weak intermolecular hydrogen bonding-like interaction between the methyl H atoms and the O atoms of the *n*-PrO groups (Figure S20 in SI). Note that two different H···O distances as such, one at 2.9±0.1 Å and the other at 3.2±0.1 Å, for inner and outer circles of CS Au_3Cb_3 are observed (see right side in Figure S20 in SI). The different H···O distances can be attributed to the *'water wheel'* shape of CS morphology. We also found that the bond angles (∠CHO) were ~ 107±10°, which are consistent with H···O bonding interactions reported for methyl groups.[91,92] Note that the hydrogen atoms that are involved in H···O bonds are not bound to an electronegative atom. Hence we describe them as hydrogen bond-like interactions, which are much weaker than traditional hydrogen bonds. Finally, the strongest interactions that are driving the close packing of the gold trimers could be the metallo-π interactions between the gold molecules and the HOPG surface.

Another very interesting feature of the Au_3Cb_3 CS morphology is the formation of a porous network (Figures 4c-4d, and Figure S15 in SI) with a pore diameter of ~ 9.5 Å. The pore is present at the center of each '*water wheel*' formed by six Au_3Cb_3 molecules per pore. The pore size is too small to allow another Au_3Cb_3 molecule to settle inside but could host smaller molecules like corannulene or pyrene. To determine whether the porous morphology of Au_3Cb_3 monolayer (Figures 4c-4d) can host a small molecule, we added an excess amount of a pyrene solution dissolved in phenyloctane solvent (10 µL of ~5×10^{-4} M) on top of the existing Au_3Cb_3 monolayer (see Sec. 2C in experimental methods). A solution cell was used to maintain the surface concentrations for all experiments involving pyrene and Au_3Cb_3. Due to its flat structure, pyrene molecules should lay flat at the center of the hexagonal closed structure (CS) morphology of Au_3Cb_3. A similar experiment was also performed with the porous structure obtained from electrochemical self-assembly of 4-nitroaniline molecules on Au(111).[90]

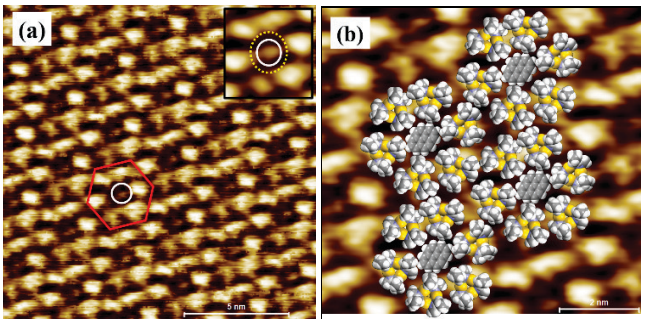

Figure 6. (a) STM image (-0.4 V and 60 pA set point) of a closed structure (CS) Au_3Cb_3 monolayer on HOPG with pyrene molecules at the center of CS. The red hexagon represent the unit cell; inset at the top right corner represents high-resolution image of each CS. The dotted yellow circle represents a nano-pore and solid white circle represents a pyrene molecule. (b) A correlation-averaged CS STM image with proposed models of Au_3Cb_3 and pyrene laid on top. Pyrene molecules can be clearly seen at the center of each CS.

Upon adding excess pyrene solution on top of the existing CS Au_3Cb_3 monolayer, the pyrene molecules appear as a dim dot at the center of the hexagonal CS (Figure 6a). The dim appearance of the pyrene molecule can be attributed to the strong tunneling of the gold atoms of Au_3Cb_3 and smaller molecular size and weak tunneling of pyrene. The appearance of pyrene on the HOPG surface is consistent with earlier STM studies of pyrene or pyrene-containing species on HOPG.[93-95] Note that a higher setpoint current of ~60 pA is needed to even see the pyrene molecules. STM images of Au_3Cb_3 monolayer on HOPG with a similar setpoint current and sample bias voltage just before adding the pyrene solution (Figure S16 in SI) clearly show a dark hole instead of a dim dot at the center of the CS. Due to the smaller size and weak tunneling of the pyrene molecule, we can only report that it lies at the center of the hexagonal CS structure but its exact orientation within the CS is not clear. Hence, the orientation of pyrene in the hexagonal CS structure in the proposed model (Figure 6b) was arbitrarily chosen. It is also possible that the pyrene molecule is rotating between symmetrically equivalent positions at the center of the pore. STM studies[96,97] have shown that the surface lattice site of the 'host' porous structure tends to change or reconstruct upon adding the guest molecule. But no such lattice site changes were observed for the Au_3Cb_3 porous/CS structure within our

ability to characterize the occupied lattice at the noise level of the present images.

Numerous porous or nanoporous structures on surfaces were reported in the literature, many of which were noted in excellent reviews by De Feyter,[1,8] Barth[2,3,23,98] and co-workers. It was noted that several interaction types -- such as covalent bonding, metal-ligand interactions with or without the role of adatoms, self-assembly through hydrogen bonding, electrostatic attractive or repulsive interactions, van der Waals forces, chirality, substrate, and medium from which molecules are adsorbed onto that substrate -- all play a critical role in directing the formation of porous networks on surfaces. Among all the studies of porous or nano-porous networks reported in the literature, all the molecules involved in the formation of a porous network are either organic or metal-organic (metals mostly ligated through nitrogen or oxygen) but none are organometallic (i.e., no metal-carbon bond). We note that there were two reported studies[99,100] that we are aware of wherein organometallic complexes form porous structures on substrates. But the molecular components (that bind/adsorb to the substrate) involved in the formation of porous structure are actually organic moieties, as opposed to the transition metal centers. The *CS morphology of Au_3Cb_3 (Figure 4c-d) is the first reported metal-directed porous morphology in any organometallic system*. Here, the gold atoms of Au_3Cb_3 complex are directly adsorbed onto the HOPG substrate and are active participants in the adsorbed porous structure. Of equal or perhaps greater importance, this porous structure is not regulated or assisted by interactions of alkane chains, covalent bonding, or strong electrostatic interactions. Another unique feature of the current study is the formation of surface host-guest network. There are a variety of host-guest systems studied with STM.[90,101-104] Host-guest interactions can be directed based on coordination,[96,103] electrostatic bonding,[103] solvent-induced,[104] simple molecular self-assembly,[90] *etc*. The *Au_3Cb_3-pyrene network (Figure 6) observed in the current study is the first reported host-guest network on the surface for any organometallic system.*

More studies are needed to fully understand this polymorphic self-assembly process and characterize the underlying optoelectronic properties. For example, the role of substrate, solvent, length of alkyl chain substituent, solute concentration, temperature, *etc.*, should be determined and will be pursued in the future. Likewise, remarkably-rich optoelectronic properties are anticipated for such binary materials akin to those known for similar systems that were not tethered to a surface.[105,106] Likewise, the absence of inter-trimer association in the monolayers of both CTCs on HOPG examined herein is in a stark contrast to the situation known for solutions and solids of the trimers alone, wherein association plays a central role in determining their optoelectronic properties; a new avenue of optoelectronics research, therefore, will be rendered by these alternative surface-bound systems wherein the activity is bestowed by trimer-surface as opposed to trimer-trimer electronic communications.

5. SUMMARY AND CONCLUSIONS

In summary, we report the synthesis, characterization and scanning tunneling microscopy imaging of two new gold(I) cyclic trinuclear complexes on phenyloctane/HOPG solution-solid interface. X-ray crystallography revealed that both gold(I) complexes have 1-dimensional stacking patterns induced by intermolecular Au(I)···Au(I) aurophilic bonding. The Au_3Pz_3 trimers stack with two alternating and symmetrical Au(I)···Au(I) interactions and the distance of the Au(I)···Au(I) interactions vary with temperature. The Au_3Cb_3 trimer stacks have three alternating and non-symmetrical Au(I)···Au(I) intermolecular bonds in each stack. Self-assembly studies at the solution-solid interface have shown that gold(I) CTCs lie flat on HOPG surface with bright triangular Au_3 centers. Independent of the solution concentration, we found that Au_3Pz_3 molecules assemble in a single morphology while Au_3Cb_3 molecules assemble as two polymorphs. Both gold(I) trimers, polymorphic or not, form an epitaxial nanostructure on HOPG. We were able to determine the lattice structures of each polymorph based on STM imaging supported by the crystal structures and molecular/periodic DFT calculations.

STM imaging revealed that Au_3Pz_3 trimers on HOPG form a 2-D hexagonal lattice with one molecule per unit cell, $a = b = 1.54$ nm and $\alpha = 60°$, with surface density of 0.487 molecules/nm^2. The ethyl ester substituents of Au_3Pz_3 trimers were determined to be lying flat on the HOPG surface and with possible surface defects where each Au_3Pz_3 trimer can be in an inverted orientation (rotated by 60°) with respect to its neighbors. The Au_3Cb_3 trimers exhibit polymorphomism on the HOPG surface at room temperature (22.0±2.0 °C), forming a non-porous, low-density (0.82 molecules/nm^2) nanostructure first and then transforming into a high-density (1.43 molecules/nm^2), porous nanostructure on the substrate. Both polymorphs of Au_3Cb_3 form epitaxial hexagonal 2-D lattice structures on HOPG with lattice parameters of $a = b = 1.48$ nm and $\alpha = 60°$ for the non-porous nanostructure and $a = b = 2.90$ nm and $\alpha = 60°$ for the porous nanostructure.

The porous polymorph formed by the $Au_3[(n\text{-Pr-O})C{=}N(Me)]_3$ carbeniate complex is the first metal-directed porous organometallic nanostructure. We were able to fill the pores with pyrene molecules making this structure the first reported host-guest organometallic system imaged on a surface. It was found that pyrene adsorbs at the center of the Au_3Cb_3 pore with no obvious distortion of the pore. The flat and epitaxial self-assembly of gold(I) CTCs on HOPG and the associated good electronic communication with the HOPG surface render these CTCs excellent choices for graphene functionalization.[47] Also, the porous morphology of the Au_3Cb_3 monolayers makes them promising molecules for controlled self-assembly process *via* the component network strategy[107,108] used for nanopatterning surfaces. Such controlled self-assembly process might ultimately lead to '*bottom-up*' fabrication of devices.

ACKNOWLEDGEMENTS:

We gratefully acknowledge support of this work by the US National Science Foundation (CHE-1112156 to UM,

CHE-1403989 to KWH, and CHE-1413641, CMMI-0963509 and CHE-0840518 to MAO). The computational work was performed using EMSL, a DOE Office of Science User Facility sponsored by the Office of Biological and Environmental Research and located at Pacific Northwest National Laboratory (PNNL). Part of the computations were also supported by resources from PNNL Institutional Computing (PIC) program at PNNL.

REFERENCES:

1. Elemans, J. A. A. W.; Lei, S.; De Feyter, S. Molecular and Supramolecular Networks on Surfaces: From Two-Dimensional Crystal Engineering to Reactivity. *Angew. Chem., Int. Ed.* **2009,** *48* (40), 7298-7332.
2. Barth, J. V. Molecular Architectonic on Metal Surfaces. *Annu. Rev. Phys. Chem.* **2007,** *58* (1), 375-407.
3. Barth, J. V.; Costantini, G.; Kern, K. Engineering atomic and molecular nanostructures at surfaces. *Nature* **2005,** *437* (7059), 671-679.
4. English, W. A.; Hipps, K. W. Stability of a Surface Adlayer at Elevated Temperature: Coronene and Heptanoic Acid on Au(111). *J. Phys. Chem. C* **2008,** *112* (6), 2026-2031.
5. MacLeod, J. M.; Rosei, F. Expanding the Scope of Molecular Self-organization Studies through Temperature Control at the Solution/Solid Interface. *Aust. J. Chem.* **2011,** *64* (9), 1299-1300.
6. Stepanow, S.; Lingenfelder, M.; Dmitriev, A.; Spillmann, H.; Delvigne, E.; Lin, N.; Deng, X.; Cai, C.; Barth, J. V.; Kern, K. Steering molecular organization and host-guest interactions using two-dimensional nanoporous coordination systems. *Nature* **2004,** *3* (4), 229-233.
7. Mali, K. S.; De Feyter, S. Principles of molecular assemblies leading to molecular nanostructures. *Philos. Trans. A Math. Phys. Eng. Sci.* **2013,** *371* (2000), pp 1-20.
8. Kudernac, T.; Lei, S.; Elemans, J. A. A. W.; De Feyter, S. Two-dimensional supramolecular self-assembly: nanoporous networks on surfaces. *Chem. Soc. Rev.* **2009,** *38* (2), 402-421.
9. Hipps, K. W.; Mazur, U. Kinetic and Thermodynamic Processes of Organic Species at the Solution Solid Interface: The view through an STM. *Chem. Comm.* **2015,** *51*, 4737-4749.
10. Theobald, J. A.; Oxtoby, N. S.; Phillips, M. A.; Champness, N. R.; Beton, P. H. Controlling molecular deposition and layer structure with supramolecular surface assemblies. *Nature* **2003,** *424* (6952), 1029-1031;
11. Hipps, K. W. Scanning Tunneling Spectroscopy. In *Handbook of Applied Solid State Spectroscopy*, Vij, D. R., Ed. **2006**.
12. Rosei, F.; Schunack, M.; Naitoh, Y.; Jiang, P.; Gourdon, A.; Laegsgaard, E.; Stensgaard, I.; Joachim, C.; Besenbacher, F. Properties of large organic molecules on metal surfaces. *Prog. Surf. Sci.* **2003,** *71* (5–8), 95-146
13. Forrest, S. R. Ultrathin Organic Films Grown by Organic Molecular Beam Deposition and Related Techniques. *Chem. Rev.* **1997,** *97* (6), 1793-1896.
14. Gutzler, R.; Cardenas, L.; Rosei, F. Kinetics and thermodynamics in surface-confined molecular self-assembly. *Chem. Sci.* **2011,** *2* (12), 2290-2300.
15. Gutzler, R.; Sirtl, T.; Dienstmaier, J. F.; Mahata, K.; Heckl, W. M.; Schmittel, M.; Lackinger, M. Reversible Phase Transitions in Self-Assembled Monolayers at the Liquid−Solid Interface: Temperature-Controlled Opening and Closing of Nanopores. *J. Am. Chem. Soc.* **2010,** *132* (14), 5084-5090.
16. Mamdouh, W.; Uji-i, H.; Ladislaw, J. S.; Dulcey, A. E.; Percec, V.; De Schryver, F. C.; De Feyter, S. Solvent Controlled Self-Assembly at the Liquid-Solid Interface Revealed by STM. *J. Am. Chem. Soc.* **2005,** *128* (1), 317-325.
17. Bhattarai, A.; Mazur, U.; Hipps, K. W. A Single Molecule Level Study of the Temperature-Dependent Kinetics for the Formation of Metal Porphyrin Monolayers on Au(111) from Solution. *J. Am. Chem. Soc.* **2014,** *136* (5), 2142-2148.
18. Friesen, B. A.; Bhattarai, A.; Mazur, U.; Hipps, K. W. Single Molecule Imaging of Oxygenation of Cobalt Octaethylporphyrin at the Solution/Solid Interface: Thermodynamics from Microscopy. *J. Am. Chem. Soc.* **2012,** *134* (36), 14897-14904.
19. Tanaka, H.; Kawai, T. Partial sequencing of a single DNA molecule with a scanning tunnelling microscope. *Nat. Nanotech.* **2009,** *4* (8), 518-522;
20. STM and AFM of bio/organic molecules and structures. *Surf. Sci. Rep.* **1996,** *26* (8), 261-332
21. Ikai, A.; Li, M. Q. Scanning probe microscopy (STM/AFM) and applications in biology. *App. Phys. A* **1999,** *68* (2), 255-258.
22. Wang, Y.; Wu, K.; Kroeger, J.; Berndt, R. Structures of phthalocyanine molecules on surfaces studied by STM. *AIP Adv.* **2012,** *2* (4), 041402, pp 1-11.
23. Broekmann, P.; Dötz, K.-H.; Schalley, C.; Lin, N.; Stepanow, S.; Ruben, M.; Barth, J. Surface-Confined Supramolecular Coordination Chemistry. In *Templates in Chemistry III*, Springer Berlin Heidelberg: **2009,** *287*, 1-44.
24. Lin, N.; Dmitriev, A.; Weckesser, J.; Barth, J. V.; Kern, K. Real-Time Single-Molecule Imaging of the Formation and Dynamics of Coordination Compounds. *Angew. Chem., Int. Ed.* **2002,** *41* (24), 4779-4783.
25. Fan, Q.; Wang, C.; Han, Y.; Zhu, J.; Kuttner, J.; Hilt, G.; Gottfried, J. M. Surface-Assisted Formation, Assembly, and Dynamics of Planar Organometallic Macrocycles and Zigzag Shaped Polymer Chains with C-Cu-C Bonds. *ACS Nano* **2014,** *8* (1), 709-718.
26 Shchyrba, A.; Wäckerlin, C.; Nowakowski, J.; Nowakowska, S.; Björk, J.; Fatayer, S.; Girovsky, J.; Nijs, T.; Martens, S. C.; Kleibert, A.; Stöhr, M.; Ballav, N.; Jung, T. A.; Gade, L. H. Controlling the Dimensionality of On-Surface Coordination Polymers via Endo- or Exoligation. *J. Am. Chem. Soc.* **2014,** *136* (26), 9355-9363.
27. Surin, M.; Samorì, P.; Jouaiti, A.; Kyritsakas, N.; Hosseini, M. W. Molecular Tectonics on Surfaces: Bottom-Up Fabrication of 1D Coordination Networks That Form 1D and 2D Arrays on Graphite. *Angew. Chem.* **2007,** *119* (1-2), 249-253.
28. Garah, M. E.; Ciesielski, A.; Marets, N.; Bulach, V.; Hosseini, M. W.; Samori, P. Molecular tectonics based nanopatterning of interfaces with 2D metal-organic frameworks (MOFs). *Chem. Comm.* **2014,** *50* (82), 12250-12253.
29. Ruben, M.; Rojo, J.; Romero-Salguero, F. J.; Uppadine, L. H.; Lehn, J.-M. Grid-Type Metal Ion Architectures: Functional Metallosupramolecular Arrays. *Angew. Chem., Int. Ed.* **2004,** *43* (28), 3644-3662.
30. Yamada, T.; Sekine, R.; Sawaguchi, T. Ultrahigh-vacuum multitechnique study of AuCN monolayers on Au(111) formed by electrochemical deposition. *J. Chem. Phys.* **2000,** *113* (3), 1217-1227.
31. Sawaguchi, T.; Yamada, T.; Okinaka, Y.; Itaya, K. Electrochemical Scanning Tunneling Microscopy and Ultrahigh-Vacuum Investigation of Gold Cyanide Adlayers on Au(111) Formed in Aqueous Solution. *J. Phys. Chem.* **1995,** *99* (38), 14149-14155.

32. Shen, J.; Jia, J.; Bobrov, K.; Guillemot, L.; Esaulov, V. Electron transfer processes on Au nanoclusters supported on graphite. *Gold Bulletin* **2013,** *46* (4), 343-347.
33. Ong, Q. K.; Zhao, S.; Reguera, J.; Biscarini, F.; Stellacci, F. Comparative STM studies of mixed ligand monolayers on gold nanoparticles in air and in 1-phenyloctane. *Chem. Comm.* **2014,** *50* (72), 10456-10459.
34. Ong, Q. K.; Reguera, J.; Silva, P. J.; Moglianetti, M.; Harkness, K.; Longobardi, M.; Mali, K. S.; Renner, C.; De Feyter, S.; Stellacci, F. High-Resolution Scanning Tunneling Microscopy Characterization of Mixed Monolayer Protected Gold Nanoparticles. *ACS Nano* **2013,** *7* (10), 8529-8539.
35. Jackson, A. M.; Myerson, J. W.; Stellacci, F. Spontaneous assembly of subnanometre-ordered domains in the ligand shell of monolayer-protected nanoparticles. *Nat. Mater.* **2004,** *3* (5), 330-336.
36. Müllegger, S.; Schöfberger, W.; Rashidi, M.; Reith, L. M.; Koch, R. Spectroscopic STM Studies of Single Gold(III) Porphyrin Molecules. *J. Am. Chem. Soc.* **2009,** *131* (49), 17740-17741.
37. Chusuei, C. C.; Lai, X.; Davis, K. A.; Bowers, E. K.; Fackler, J. P.; Goodman, D. W. A Nanoscale Model Catalyst Preparation: Solution Deposition of Phosphine-Stabilized Gold Clusters onto a Planar TiO2(110) Support. *Langmuir* **2001,** *17* (13), 4113-4117.
38. Omary. M. A.; Rawashdeh-Omary, M. A.; Chusuei, C. C.; Fackler, J. P., Jr.; Bagus, P. S. Electronic Structure Studies of Six-atom Gold Clusters. *J. Chem. Phys.* **2001**, *114*, 10695-10701.
39. den Boer, D.; Krikorian, M.; Esser, B.; Swager, T. M. STM Study of Gold(I) Pyrazolates: Distinct Morphologies, Layer Evolution, and Cooperative Dynamics. *J. Phys. Chem. C* **2013,** *117* (16), 8290-8298.
40. Omary, M. A.; Rawashdeh-Omary, M.; Gonser, M. W. A.; Elbjeirami, O.; Grimes, T.; Cundari, T. R.; Diyabalanage, H. V. K.; Gamage, C. S. P.; Dias, H. V. R. Metal Effect on the Supramolecular Structure, Photophysics, and Acid-Base Character of Trinuclear Pyrazolato Coinage Metal Complexes. *Inorg. Chem.* **2005,** *44* (23), 8200-8210.
41. White-Morris, R.; Olmstead, M. M.; Attar, S.; Balch, A. L. Intermolecular Interactions in Polymorphs of Trinuclear Gold(I) Complexes: Insight into the Solvoluminescence of AuI3(MeNC═OMe)3. *Inorg. Chem.* **2005,** *44* (14), 5021-5029.
42. McDougald, R. N.; Chilukuri, B.; Jia, H.; Perez, M. R.; Rabaâ, H.; Wang, X.; Nesterov, V. N.; Cundari, T. R.; Gnade, B. E.; Omary, M. A. Molecular and Electronic Structure of Cyclic Trinuclear Gold(I) Carbeniate Complexes: Insights for Structure/Luminescence/Conductivity Relationships. *Inorg. Chem.* **2014,** *53* (14), 7485-7499.
43. Zhu, L.; Coropceanu, V.; Yi, Y.; Chilukuri, B.; Cundari, T. R.; Brédas, J.-L. Electronic and Charge-Transport Properties of the Au3(CH3N═COCH3)3 Crystal: A Density Functional Theory Study. *J. Phys. Chem. Lett.* **2013,** *4* (13), 2186-2189.
44. Galassi, R.; Ricci, S.; Burini, A.; Macchioni, A.; Rocchigiani, L.; Marmottini, F.; Tekarli, S. M.; Nesterov, V. N.; Omary, M. A. Solventless Supramolecular Chemistry via Vapor Diffusion of Volatile Small Molecules upon a New Trinuclear Silver(I)-Nitrated Pyrazolate Macrometallocyclic Solid: An Experimental /Theoretical Investigation of the Dipole/Quadrupole Chemisorption Phenomena. *Inorg. Chem.* **2013,** *52* (24), 14124-14137.
45. Moon, J. S.; Curtis, D.; Hu, M.; Wong, D.; McGuire, C.; Campbell, P. M.; Jernigan, G.; Tedesco, J. L.; VanMil, B.; Myers-Ward, R.; Eddy, C.; Gaskill, D. K. Epitaxial-Graphene RF Field-Effect Transistors on Si-Face 6H-SiC Substrates. IEEE *Electr. Device L.* **2009,** *30* (6), 650-652.
46. Wang, X.; Tabakman, S. M.; Dai, H. Atomic Layer Deposition of Metal Oxides on Pristine and Functionalized Graphene. *J. Am. Chem. Soc.* **2008,** *130* (26), 8152-8153.
47. Huang, H.; Chen, S.; Gao, X.; Chen, W.; Wee, A. T. S. Structural and Electronic Properties of PTCDA Thin Films on Epitaxial Graphene. *ACS Nano* **2009,** *3* (11), 3431-3436.
48. Dong, X.; Fu, D.; Fang, W.; Shi, Y.; Chen, P.; Li, L.-J. Doping Single-Layer Graphene with Aromatic Molecules. *Small* **2009,** *5* (12), 1422-1426.
49. Dong, X.; Shi, Y.; Zhao, Y.; Chen, D.; Ye, J.; Yao, Y.; Gao, F.; Ni, Z.; Yu, T.; Shen, Z.; Huang, Y.; Chen, P.; Li, L.-J. Symmetry Breaking of Graphene Monolayers by Molecular Decoration. *Phys. Rev. Lett.* **2009,** *102* (13), 135501.
50. Qi, Y.; Mazur, U.; Hipps, K. W. Charge transfer induced chemical reaction of tetracyano-p-quinodimethane adsorbed on graphene. *RSC Adv.* **2012,** *2* (28), 10579-10584.
51. Tekarli, S. M.; Cundari, T. R.; Omary, M. A. Rational Design of Macrometallocyclic Trinuclear Complexes with Superior pi-Acidity and pi-Basicity. *J. Am. Chem. Soc.* **2008,** *130* (5), 1669-1675.
52. Kishimura, A.; Yamashita, T.; Aida, T. Phosphorescent Organogels via "Metallophilic" Interactions for Reversible RGB−Color Switching. *J. Am. Chem. Soc.* **2005,** *127* (1), 179-183.
53. Casanova, J.; Schuster, R. E.; Werner, N. D. Synthesis of Aliphatic Isocyanides. *J. Chem. Soc. (Resumed)* **1963**, 4280.
54. Usón, R.; Laguna, A. Polyaryl Derivatives Of Gold(I), Silver(I) and Gold(III). *Organomet. Synth.* **1986,** *3*, 322-342.
55. Murray, H. H.; Raptis, R. G.; Fackler, J. P. Syntheses and x-ray structures of group 11 pyrazole and pyrazolate complexes. X-ray crystal structures of bis(3,5-diphenylpyrazole)copper(II) dibromide, tris(.mu.-3,5-diphenylpyrazolato-N,N')trisilver(I)-2-tetrahydrofuran, tris(.mu.-3,5-diphenylpyrazolato-N,N')trigold(I), and hexakis(.mu.-3,5-diphenylpyrazolato-N,N')hexagold(I). *Inorg. Chem.* **1988,** *27* (1), 26-33.
56. Parks, J. E.; Balch, A. L. Gold carbene complexes: preparation, oxidation, and ligand displacement. *J. Organomet. Chem.* **1974,** *71* (3), 453-463.
57. Bruker APEX2; Bruker AXS Inc.: Madison, WI. **2007**.
58. Bruker SAINT; Bruker AXS Inc.: Madison, WI. **2007**.
59. Bruker SADABS; Bruker AXS Inc.: Madison, WI. **2007**.
60. Sheldrick, G. M. SHELXTL. **2008**.
61. *SPIP*, Image Metrology: Hørsholm, Denmark.
62. Tong, W. Ph.D. Thesis: Controlling Self-Assembled Monolayer Morphology with Dipolar Interactions: Preparation, STM Image Analysis and Simulations of 1,5-(Disubstituted)-Anthracene Monolayers. Brown University, Providence, RI, **2010**.
63. Frisch, M. J.; et. al Gaussian 09, Revision A.1; Gaussian, Inc.: Wallingford, CT, **2009**.
64. Hay, P.; Wadt, W. Ab initio effective core potentials for molecular calculations. Potentials for the transition metal atoms Sc to Hg. In *J. Chem. Phys.* **1985,** *82*, 270-283.
65. Zhao, Y.; Truhlar, D. The M06 suite of density functionals for main group thermochemistry, thermochemical kinetics, noncovalent interactions, excited states, and transition elements: two new functionals and systematic testing of four M06-class functionals and 12 other functionals. *Theor. Chem. Account* **2008,** *120* (1), 215-241.
66. Pyykkö, P.; Mendizabal, F. Theory of d10−d10 Closed-Shell Attraction. III. Rings. *Inorg. Chem.* **1998,** *37* (12), 3018-3025.

67. Couty, M.; Hall, M. B. Basis sets for transition metals: Optimized outer p functions. *J. Comput. Chem.* **1996,** *17* (11), 1359-1370.
68. Chilukuri, B.; Cundari, T. R. Modeling the Deposition of Metal Atoms on a p-Type Organometallic Conductor: Implications for Stability and Electron Transfer. *J. Phys. Chem. C* **2011,** *115* (13), 5997-6003.
69. Kresse, G.; Furthmüller, J. Efficiency of ab-initio total energy calculations for metals and semiconductors using a plane-wave basis set. *Comp. Mater. Sci.* **1996,** *6* (1), 15-50.
70. Kresse, G.; Furthmüller, J. Efficient iterative schemes for ab initio total-energy calculations using a plane-wave basis set. *Phys. Rev. B* **1996,** *54* (16), 11169.
71. Kresse, G.; Hafner, J. Ab initio molecular dynamics for liquid metals. *Phys. Rev. B* **1993,** *47* (1), 558-561.
72. Kresse, G.; Joubert, D. From ultrasoft pseudopotentials to the projector augmented-wave method. *Phys. Rev. B* **1999,** *59* (3), 1758
73. Blöchl, P. E. Projector augmented-wave method. *Phys. Rev. B* **1994,** *50* (24), 17953.
74. Klimeš, J.; Bowler, D. R.; Michaelides, A. Van der Waals density functionals applied to solids. *Phys. Rev. B* **2011,** *83* (19), 195131.
75. Lee, K.; Murray, É. D.; Kong, L.; Lundqvist, B. I.; Langreth, D. C. Higher-accuracy van der Waals density functional. *Phys. Rev. B* **2010,** *82* (8), 081101.
76. Jiří Klimeš and David, R. B.; Michaelides, A. Chemical accuracy for the van der Waals density functional. *J. Phys. Condens. Matter* **2010,** *22* (2), 022201.
77. Chilukuri, B.; Mazur, U.; Hipps, K. W. Effect of dispersion on surface interactions of cobalt(ii) octaethylporphyrin monolayer on Au(111) and HOPG(0001) substrates: a comparative first principles study. *Phys. Chem. Chem. Phys.* **2014,** *16* (27), 14096-14107.
78. Monkhorst, H. J.; Pack, J. D. Special points for Brillouin-zone integrations. *Phys. Rev. B* **1976,** *13* (12), 5188.
79. Tersoff, J.; Hamann, D. R. Theory of the scanning tunneling microscope. *Phys. Rev. B* **1985,** *31* (2), 805-813.
80. Tersoff, J.; Hamann, D. R. Theory and Application for the Scanning Tunneling Microscope. *Phys. Rev. Lett.* **1983,** *50* (25), 1998-2001.
81. Krisztián Palotás and Werner, A. H. Multiple scattering in a vacuum barrier obtained from real-space wavefunctions. *J. Phys. Condens. Matter* **2005,** *17* (17), 2705.
82. Vickery, J. C.; Olmstead, M. M.; Fung, E. Y.; Balch, A. L. Solvent-Stimulated Luminescence from the Supramolecular Aggregation of a Trinuclear Gold(I) Complex that Displays Extensive Intermolecular Au...Au Interactions. *Angew. Chem., Int. Ed. in English* **1997,** *36* (11), 1179-1181.
83. Pyykkö, P.; Li, J.; Runeberg, N. Predicted ligand dependence of the Au(I)...Au(I) attraction in (XAuPH3)2. *Chem. Phys. Lett.* **1994,** *218* (1-2), 133-138.
84. Chilukuri, B.; Cundari, T. R. Surface interactions of Au(I) cyclo-trimer with Au(111) and Al(111) surfaces: A computational study. *Surf. Sci.* **2012,** *606* (13-14), 1100-1107.
85. Burgess, A. W.; Shipman, L. L.; Scheraga, H. A. A new approach to empirical intermolecular and conformational potential energy functions. II. Applications to crystal packing, rotational barriers, and conformational analysis. *Proc. Natl. Acad. Sci. U.S.A.* **1975,** *72* (3), 854-8.
86. Jahanbekam, A.; Vorpahl, S.; Mazur, U.; Hipps, K. W. Temperature Stability of Three Commensurate Surface Structures of Coronene Adsorbed on Au(111) from Heptanoic Acid in the 0 to 60°C Range. *J. Phys. Chem. C* **2013,** *117* (6), 2914-2919.
87. Blunt, M. O.; Adisoejoso, J.; Tahara, K.; Katayama, K.; Van der Auweraer, M.; Tobe, Y.; De Feyter, S. Temperature-Induced Structural Phase Transitions in a Two-Dimensional Self-Assembled Network. *J. Am. Chem. Soc.* **2013,** *135* (32), 12068-12075.
88. Bellec, A.; Arrigoni, C.; Schull, G.; Douillard, L.; Fiorini-Debuisschert, C.; Mathevet, F.; Kreher, D.; Attias, A.-J.; Charra, F. Solution-growth kinetics and thermodynamics of nanoporous self-assembled molecular monolayers. *J. Chem. Phys.* **2011,** *134* (12), 124702.
89. Goodman, L.; Pophristic, V. Where does the dimethyl ether internal rotation barrier come from?. *Chem. Phys. Lett.* **1996,** *259* (3–4), 287-295.
90. Yang, L.; Wang, D.; Wan, L.-J. Formation of host–guest structure at an electrified electrode surface: An electrochemical STM investigation. *Electrochem Commun* **2012,** *17*, 82-84.
91. Knak Jensen, S. J.; Tang, T.-H.; Csizmadia, I. G. Hydrogen-Bonding Ability of a Methyl Group. *J. Phys. Chem. A* **2003,** *107* (42), 8975-8979.
92. Dem'yanov, P. I.; Gschwind, R. M. Formation of Hydrogen Bonds in Complexes between Dimethylcuprate(I) Anion and Methane, Propane, or Dimethyl Ether. A Theoretical Study. *Organometallics* **2006,** *25* (24), 5709-5723.
93. Zhang, X.-m.; Wang, H.-f.; Wang, S.; Shen, Y.-t.; Yang, Y.-l.; Deng, K.; Zhao, K.-q.; Zeng, Q.-d.; Wang, C. Triphenylene Substituted Pyrene Derivative: Synthesis and Single Molecule Investigation. *J. Phys. Chem. C* **2013,** *117* (1), 307-312.
94. Uji-i, H.; Nishio, S.; Fukumura, H. Electronic properties of a π-stacked pyrene derivative at a liquid–solid interface studied with scanning tunneling spectroscopy. *Chem. Phys. Lett.* **2005,** *408* (1–3), 112-117.
95. Tchebotareva, N.; Yin, X.; Watson, M. D.; Samorì, P.; Rabe, J. P.; Müllen, K. Ordered Architectures of a Soluble Hexa-peri-hexabenzocoronene−Pyrene Dyad: Thermotropic Bulk Properties and Nanoscale Phase Segregation at Surfaces. *J. Am. Chem. Soc.* **2003,** *125* (32), 9734-9739.
96. Li, Y.; Liu, C.; Xie, Y.; Li, X.; Fan, X.; Yuan, L.; Zeng, Q. Single-molecule observation of the K+-induced switching of valinomycin within a template network. *Chem. Comm.* **2013,** *49* (79), 9021-9023.
97. Zeng, X.; Chang, S.; Deng, K.; Zhang, J.; Sun, H.; Zeng, Q.; Xie, J. Synthesis and Molecular Structures of BINOL Complexes: An STM Investigation of 2D Self-Assembly. *Cryst. Growth Des.* **2015,** *15* (7), 3096-3100.
98. Barth, J. V. Fresh perspectives for surface coordination chemistry. *Surf. Sci.* **2009,** *603* (10–12), 1533-1541.
99. Wasio, N. A.; Quardokus, R. C.; Forrest, R. P.; Lent, C. S.; Corcelli, S. A.; Christie, J. A.; Henderson, K. W.; Kandel, S. A. Self-assembly of hydrogen-bonded two-dimensional quasicrystals. *Nature* **2014,** *507* (7490), 86-89.
100. Li, S.-S.; Northrop, B. H.; Yuan, Q.-H.; Wan, L.-J.; Stang, P. J. Surface Confined Metallosupramolecular Architectures: Formation and Scanning Tunneling Microscopy Characterization. *Acc. Chem. Res.* **2009,** *42* (2), 249-259.
101. Xu, J.; Zeng, Q. Two-dimensional (2D) Supramolecular Coordination at Liquid/Solid Interfaces Studied by Scanning Tunneling Microscopy. *Chin. J. Chem.* **2015,** *33* (1), 53-58.
102. Meier, C.; Landfester, K.; Künzel, D.; Markert, T.; Groß, A.; Ziener, U. Hierarchically Self-Assembled Host–Guest Network at the Solid–Liquid Interface for Single-Molecule Manipulation. *Angew. Chem., Int. Ed.* **2008,** *47* (20), 3821-3825.

103. Bertrand, H.; Silly, F.; Teulade-Fichou, M.-P.; Tortech, L.; Fichou, D. Locking the free-rotation of a prochiral star-shaped guest molecule inside a two-dimensional nanoporous network by introduction of chlorine atoms. *Chem. Comm.* **2011,** *47* (36), 10091-10093.
104. Liu, J.; Zhang, X.; Yan, H.-J.; Wang, D.; Wang, J.-Y.; Pei, J.; Wan, L.-J. Solvent-Controlled 2D Host−Guest (2,7,12-Trihexyloxytruxene/Coronene) Molecular Nanostructures at Organic Liquid/Solid Interface Investigated by Scanning Tunneling Microscopy. *Langmuir* **2010,** *26* (11), 8195-8200.
105. Elbjeirami, O.; Rawashdeh-Omary, M. A.; Omary, M. A. Phosphorescence sensitization via heavy-atom effects in d10 complexes. *Res Chem Intermediat* **2011,** *37* (7), 691-703.
106. Rawashdeh-Omary, M. A. Remarkable Alteration of Photophysical Properties of Cyclic Trinuclear Complexes of Monovalent Coinage Metals upon Interactions with Small Organic Molecules. *Comments Inorg. Chem.* **2012,** *33* (3-4), 88-101.
107. Adisoejoso, J.; Tahara, K.; Okuhata, S.; Lei, S.; Tobe, Y.; De Feyter, S. Two-Dimensional Crystal Engineering: A Four-Component Architecture at a Liquid–Solid Interface. *Angew. Chem.* **2009,** *121* (40), 7489-7493.
108. Tahara, K.; Yamaga, H.; Ghijsens, E.; Inukai, K.; Adisoejoso, J.; Blunt, M. O.; De Feyter, S.; Tobe, Y. Control and induction of surface-confined homochiral porous molecular networks. *Nat. Chem.* **2011,** *3* (9), 714-719.